Contents lists available at ScienceDirect

Transactions of Nonferrous Metals Society of China

36(2026) 628−637

www.tnmsc.cn

Kinetics and morphological evolution mechanism of WO_3 during non-isothermal hydrogen reduction

Rui-fang WANG [a,b,c], Xiang ZHAN [a,b], Yong-qiang CHEN [a,b], Shi-ming ZHANG [a,b], Yu-si CHE [a,b,c,*], Ji-lin HE [a,b,c]

[a] Zhongyuan Critical Metals Laboratory, Zhengzhou University, Zhengzhou 450001, China;

[b] National Key Laboratory for Special Rare Metal Materials, Zhengzhou University, Zhengzhou 450001, China;

[c] School of Materials Science and Engineering, Zhengzhou University, Zhengzhou 450001, China

Abstract: The hydrogen reduction kinetics of tungsten trioxide (WO_3) was investigated via non-isothermal thermogravimetric analysis. Under the local gas–solid reduction conditions, the particle morphology of tungsten powders was found to be consistent with that of raw material WO_3. The removal of oxygen from tungsten oxide during hydrogen reduction led to the formation of porous structures between the reduced particles, which were obviously different from the polyhedral single-crystal configuration of tungsten powders obtained via chemical vapor deposition. Moreover, the two-stage hydrogen reduction mechanisms of WO_3 under the local gas–solid reduction conditions can be described using the composite autocatalytic function. The activation energies of the first and second stages of the hydrogen reduction of WO_3 were determined to be 121 and 135 kJ/mol, respectively.

Keywords: tungsten trioxide; tungsten powder; hydrogen reduction; reaction kinetics; particle morphology

1 Introduction

Tungsten possesses outstanding properties such as high melting point, excellent hardness, high density, strong corrosion and wear resistance, and good electrical and thermal conductivity [1−3]. For this reason, tungsten is a strategic rare metal that plays an indispensable role in cemented carbides and electronics, as well as in chemical, medical, military, and aerospace industries [4,5]. The particle morphology of tungsten powder is an important characteristic that significantly affects its application scenarios [6−8], which depends on the reaction kinetics during the preparation process [9−11]. In industrial production of tungsten powder, the hydrogen reduction of tungsten oxides has become the mainstream method owing to the mature technic, simple equipment, and cost effectiveness of the process [12−14].

The kinetics analysis and mechanism of the hydrogen reduction of tungsten oxides are the important criteria for gaining insight into the intrinsic laws of the reduction course, which can ensure production efficiency and reduce energy consumption. For instance, SONG et al [15] proposed three mechanisms for the hydrogen reduction of tungsten oxide, namely, the adsorption-autocatalytic reaction, solid-state oxygen migration, and chemical vapor deposition. The current kinetic models describing the redox reactions, including Jander, Ginstling–Brounshtein, and Valensi–Carter models have been shown to provide guidance for practical industrial production [15]. JIANG et al [16] found two reaction mechanisms, namely solid-state oxygen migration and chemical vapor deposition, which were involved in the hydrogen reduction of tungsten oxides. In particular, geometric contraction

Corresponding author: *Yu-si CHE, Tel: +86-18737172937, E-mail: cheys@zzu.edu.cn

https://doi.org/10.1016/S1003-6326(25)66986-X

Received 17 June 2024; accepted 13 May 2025

model is a frequently applied reaction kinetic model for describing the hydrogen reduction of tungsten oxides based on the gas–solid reaction type.

To date, several studies on the morphology control of tungsten powder and kinetics of hydrogen reduction of tungsten oxide have been reported separately [17,18]. However, the correlation between the morphological evolution of tungsten powder and the kinetics of hydrogen reduction process remains unclear.

Therefore, in this study, the non-isothermal kinetic study was carried out on the hydrogen reduction of tungsten trioxides (WO_3) by using Netzsch Kinetics Neo software. Special attention was paid to gaining an in-depth understanding of the intrinsic laws of the reduction reaction by acquiring the kinetic parameters and reaction mechanisms of the hydrogen reduction of tungsten oxides. These results can supplement the morphological characteristics of tungsten powder obtained under specific reaction mechanism, thus providing a new perspective for regulating the morphological evolution behavior of tungsten powder during the reduction process.

2 Experimental

2.1 Materials

Tungsten oxides (99.9% purity) provided by Admas were used as the raw materials. Figure 1 shows the X-ray diffraction (XRD) patterns and scanning electron microscopy (SEM) image of these oxides, revealing that tungsten oxides possessed various particle sizes and WO_3 structures (corresponding to PDF #83-0950). The average particle size was measured using a Fisher Sub-sieve sizer (FSSS, WLLP−208A, China) and was found to be 9.4 μm. The ultra-pure hydrogen (purity: ≥99.99996%) produced using a hydrogen generator was employed to reduce WO_3 and to prepare tungsten powder.

2.2 Methods

A simultaneous thermal analyzer (thermo-gravimetry–differential scanning calorimetry–mass spectrometry (TG-DSC-MS), STA 449 F3 Jupiter; Germany) was used to measure the mass variation in raw powders during the hydrogen reduction of WO_3. Figure 2 illustrates the schematic diagram of the simultaneous thermal analyzer. Under the hydrogen atmosphere, a briquette of WO_3 powders was heated at specific heating rates in an alumina crucible with the diameter of 6.4 mm and the height of 14.5 mm. The measurement conditions are listed in Table 1. The mass changes of the material in the crucible at

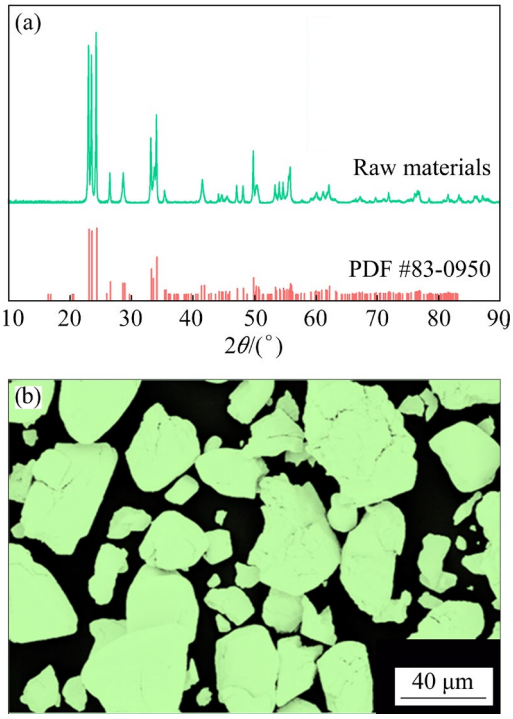

Fig. 1 XRD pattern (a) and SEM image (b) of raw materials

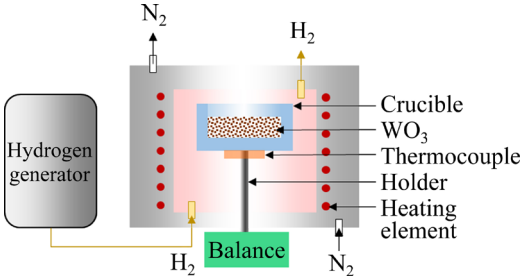

Fig. 2 Schematic diagram of simultaneous thermal analyzer

Table 1 Measurement conditions of simultaneous thermal analyzer

No.	Heating rate/(°C·min^{-1})	Initial WO_3 mass/mg	Hydrogen flow rate/(mL·min^{-1})
1	5	13.70	50
2	10	13.42	50
3	15	13.54	50
4	20	14.34	50
5	25	14.41	50

increasing temperature were recorded using a balance system in which the holder was related to the accuracy of the mass data collected. Noteworthy, the regular Pt holder may encounter hydrogen embrittlement at high temperatures, which limits the application of the simultaneous thermal analyzer in the hydrogen reduction process. To address this issue, a W–Re holder was adopted in the present study.

The mass variations were analyzed by using the Kinetics Neo software to elucidate the temperature-dependent chemical reaction kinetics and to establish a suitable kinetic model for the chemical reaction system. Equation (1) expresses the reaction for the preparation of tungsten powder by the hydrogen reduction of tungsten oxides. The conversion rate of the hydrogen reduction of WO_3 is defined as the ratio of the mass loss rate of tungsten oxides to the theoretical mass loss rate from WO_3 to W. According to Eq. (1), the theoretical mass loss rate of the solid powders should be approximately 20.7% when WO_3 is completely reduced to W.

$$WO_3+3H_2(g)=W+3H_2O(g) \quad (1)$$

3 Results and discussion

3.1 Local gas–solid hydrogen reduction mechanism of WO_3

Figure 3 depicts the mass variations in the solid powders at various heating rates during the hydrogen reduction of tungsten oxide. Figure 3(a) shows the TG plots, indicating that the hydrogen reduction of tungsten oxides proceeded in the temperature range of 430−850 °C. The mass loss approached the maximum at 850 °C, which was roughly equivalent to the theoretical mass loss rate (20.7%) of the reduction of WO_3 to W. A series of DTG curves in Fig. 3(b) reveal the change rate in the mass fraction (dw/dt) of solid powders with temperature, in which the two distinguishable features indicate that the hydrogen reduction of WO_3 proceeded in two distinct phases. A split observed between the peaks in the DTG curves corresponded to the transition temperature, which increased with the increase in the heating rate. Correspondingly, the mass loss and reaction time at the split between the peaks decreased.

Figure 4 displays the conversion rates calculated from the mass loss of the solid powders measured with the simultaneous thermal analyzer. The results indicate that the conversion rates at the same temperature decreased with increasing heating rate, which was possibly caused by a limited dynamic condition at faster heating rate. The correlation between the conversion rate and temperature provides essential information for establishing the kinetic model of the hydrogen reduction of tungsten oxide. Previous studies [19−22] have shown that WO_3 is reduced as follows: WO_3 →

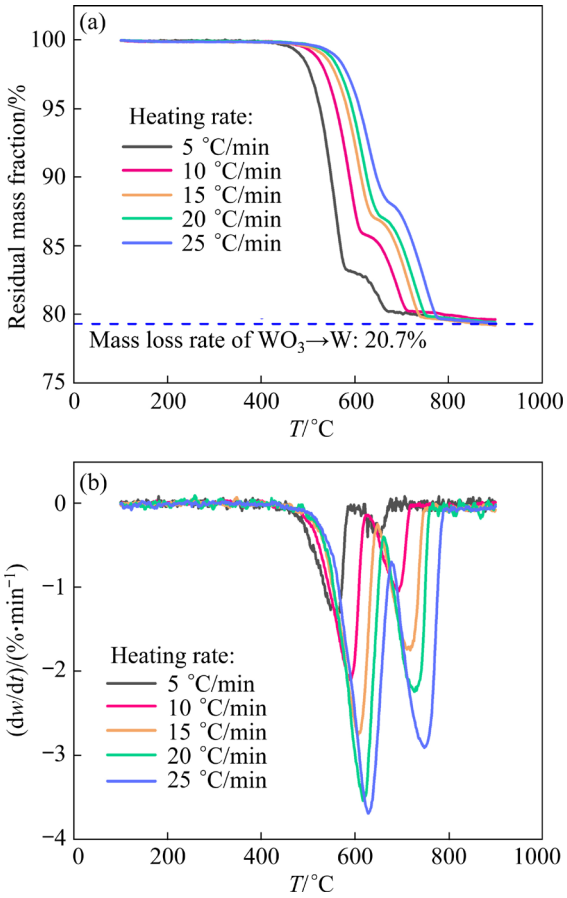

Fig. 3 Mass change of solid powders at various heating rates: (a) TG curves; (b) DTG curves

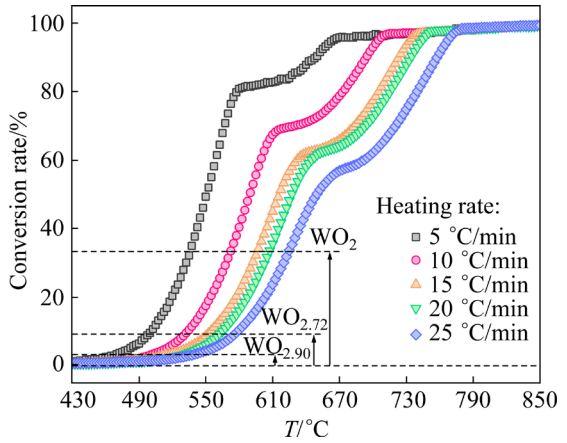

Fig. 4 Correlation between conversion rate and temperature

$WO_{2.90}$ → $WO_{2.72}$ → WO_2 → W. Therefore, the conversion rates from WO_3 to WO_x (x=2.90, 2.72, and 2) are highlighted in Fig. 4.

According to the SEM−EDS results, the intermediate products of the hydrogen reduction of WO_3 were found to be the mixtures with various proportions of WO_3, $WO_{2.90}$, $WO_{2.72}$, WO_2, and W upon the heating rate. When the hydrogen reduction reaction proceeded, oxygen contents in the intermediate products decreased. At the first stage, the main reaction was WO_3 → $WO_{2.90}$ → $WO_{2.72}$ → WO_2. In turn, the second stage primarily involved the completion of WO_x → W transformation.

Figure 5 depicts the morphology of tungsten oxides during the hydrogen reduction process. When the temperature was increased to 490 °C (Fig. 5(a)), the morphology of oxide particles did not change compared with that of WO_3. When the temperature was increased to 550 °C, the oxide particles evolved into a porous structure (Fig. 5(b)) owing to the release of water vapor formed during the hydrogen reduction of tungsten oxide. The porous structure provided channels for the hydrogen diffusion toward the unreacted tungsten oxide inside the particle. Moreover, the abundant water vapor released from the interior of the particles caused some of the oxide particles to break into fragments (Fig. 5(c)). As soon as the reaction proceeded to the interior of the particles, sintering of the products on the surface led to the decrease in the porosity relative to that inside the particles. Moreover, the tungsten powders composed of fine grains exhibited the particle morphology similar to that of WO_3. The inheritance of the W particle morphology from WO_3 could be attributed to the local gas–solid reduction (Fig. 6), whereby oxygen was removed from the WO_3 particle and W remained as the original particle [16].

Figure 7 displays the morphology of tungsten powders obtained via different reaction mechanisms using WO_3 as the raw materials. As aforementioned,

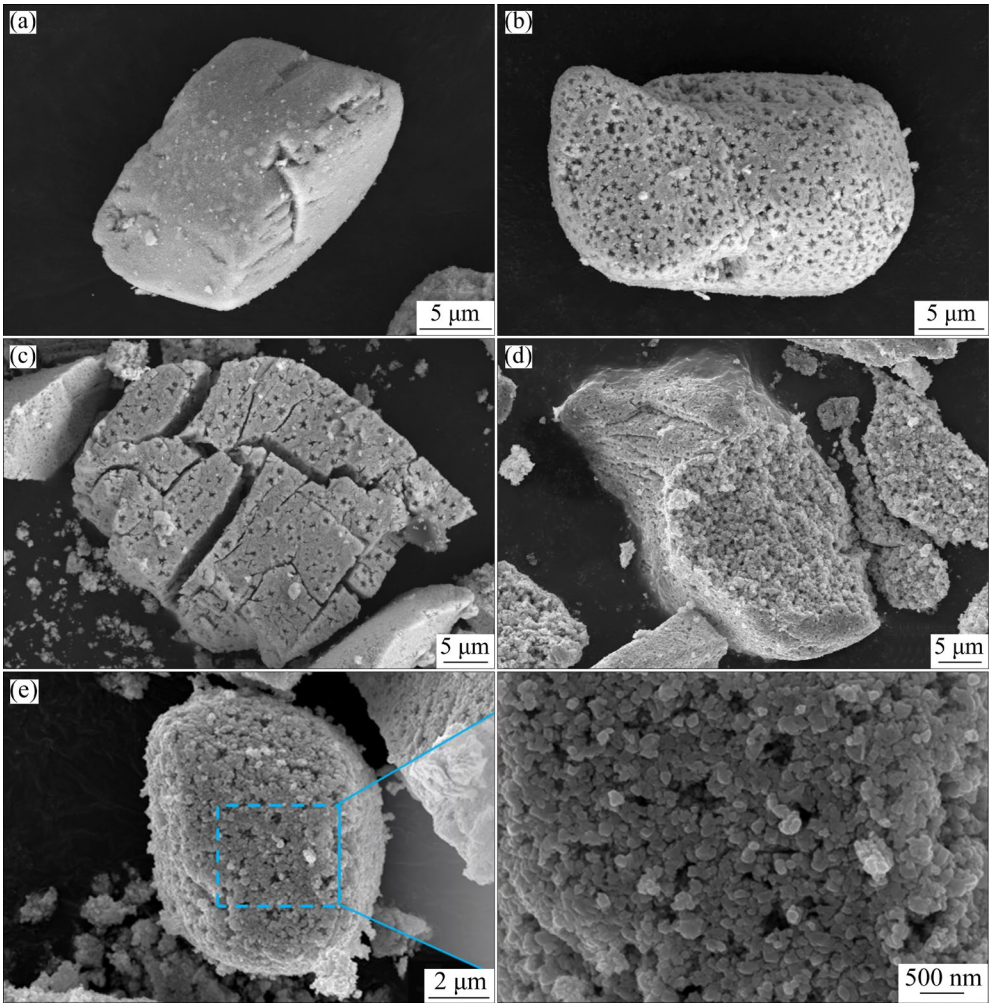

Fig. 5 SEM images of tungsten oxides upon hydrogen reduction at heating rate of 5 °C/min: (a) 490 °C; (b) 550 °C; (c) 610 °C; (d) 670 °C; (e) 790 °C

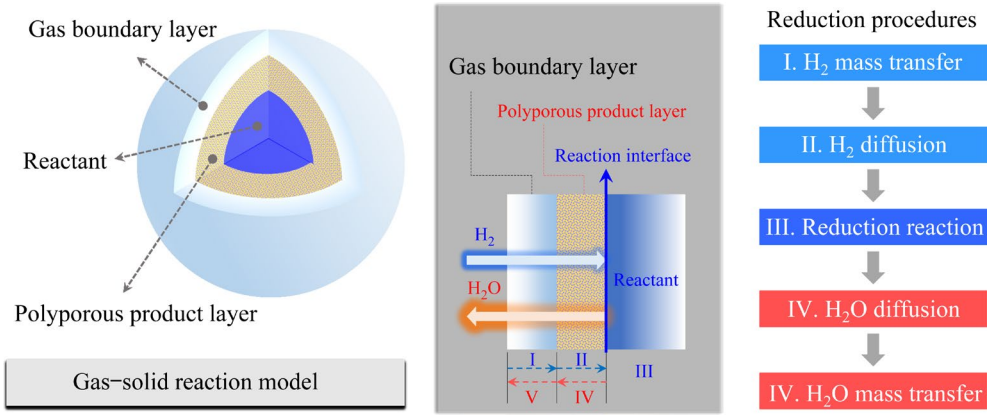

Fig. 6 Schematic diagram of local gas–solid hydrogen reduction model

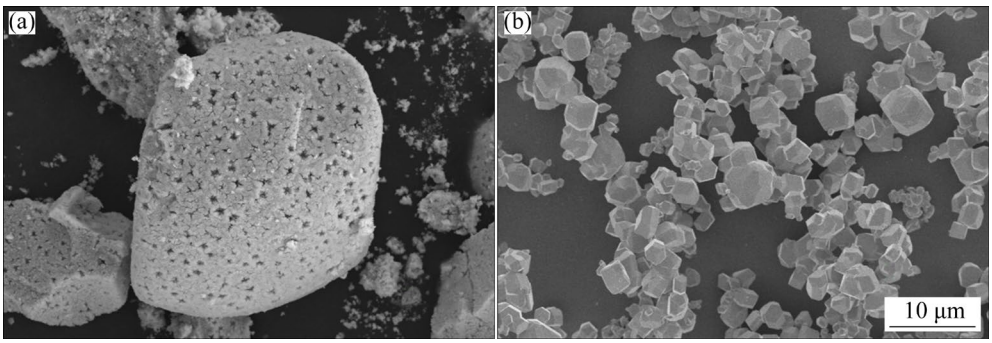

Fig. 7 Morphology of tungsten powders prepared under various reaction conditions: (a) Local gas–solid reduction; (b) Chemical vapor deposition

the powders obtained under the local gas–solid reduction conditions exhibited the morphology consistent with that of WO_3 (Fig. 7(a)). Nevertheless, the tungsten powders produced via chemical vapor deposition in the previous studies [23,24] possessed a distinct appearance (Fig. 7(b)). In a thick material, water vapor is generated by the reduction reaction (Eq. (2)), which then reacts with WO_x to produce the volatile $WO_2(OH)_2$ compound (Eq. (3)) [25−27]:

$$WO_3+(3-x)H_2(g)=WO_x(s)+(3-x)H_2O(g) \quad (2)$$

$$WO_x+(4-x)H_2O(g)=WO_2(OH)_2(g)+(3-x)H_2(g) \quad (3)$$

Figure 7(b) illustrates that tungsten with the polyhedral single-crystal structure is formed via the reduction of $WO_2(OH)_2$ conforming to the equation presented below:

$$WO_2(OH)_2(g)+3H_2(g)\rightarrow W+4H_2O(g) \quad (4)$$

Therefore, it can thus be concluded that the morphology of tungsten powders is highly dependent on the reduction reaction mechanism. In this study, the hydrogen reduction of WO_3 is quantitatively described under the local gas–solid reduction conditions based on the thermal analysis data (Fig. 4).

3.2 Kinetics analysis of hydrogen reduction of WO_3

The conversion rate of a chemical reaction can be expressed as follows:

$$\frac{d\alpha}{dt}=f(\alpha)\cdot k \quad (5)$$

where α denotes the conversion rate (%); t is the reaction time (s); $f(\alpha)$ is a mathematical function of conversion rate showing the reaction mechanism; k stands for the rate constant of the chemical reaction (s^{-1}), which can be determined from the Arrhenius equation as follows:

$$k=A\exp\left(-\frac{E_a}{RT}\right) \quad (6)$$

where A denotes the pre-exponential factor; E_a is the apparent activation energy (kJ/mol); T is the temperature (K).

The apparent activation energy is an extremely important parameter in the kinetic model. The model-free (iso-conversional) methods are used to calculate the activation energy based on a fixed conversion rate at various heating rates without assuming the reaction mechanism function. The

popular models include Friedman, Kissinger–Akahira–Sunose (KAS), ASTM E698, ASTM E2980, ASTM E2070, and Ozawa methods. Among these models, Friedman method is a classical differential iso-conversional model, whereas KAS is an integral iso-conversional approach. Figure 8 depicts the activation energy calculated by using the Friedman method and KAS model, exhibiting fluctuations within a certain range. Table 2 displays the corresponding average activation energy values. For the same reaction stage, the average activation energies obtained via the Friedman method and the KAS model were found to be close to each other.

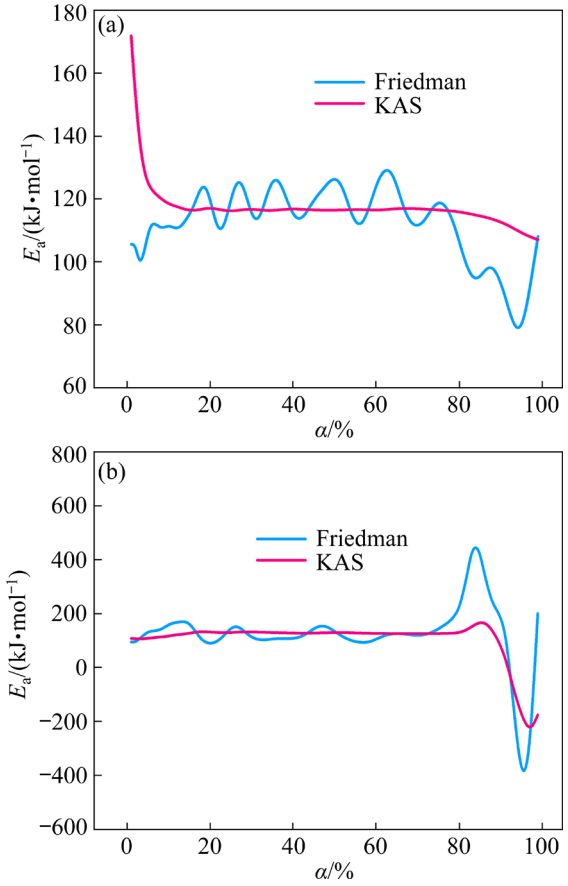

Fig. 8 Correlation between activation energy and conversion rate: (a) First stage; (b) Second stage

Table 2 Average values of activation energy calculated by model-free methods (kJ/mol)

Stage	Friedman method	KAS method
First	112	123
Second	117	104

Various functional forms have been used to describe the chemical reactions under varying mechanisms. Based on the reaction mechanism functions listed in Table 3 [28−32], this investigation attempted to distinguish the two stages of the hydrogen reduction process of tungsten oxides by employing the optimal matching method. It was found that both reaction stages could be explained in terms of the composite autocatalytic reaction mechanism. Figure 9 demonstrates that the composite autocatalytic reaction model enabled the achievement of satisfactory fitting results. The values of apparent activation energy (Fig. 10), determined from the fitting data, were close to those of model-free methods, which proves the applicability of the composite autocatalytic reaction mechanism in interpreting the hydrogen reduction of tungsten oxides.

Table 3 Reaction mechanisms and mechanism functions [28−32]

No.	Reaction mechanism	Mechanism function, $f(\alpha)$
1	Order reaction	$(1-\alpha)$
2	Order reaction	$(1-\alpha)^2$
3	Order reaction	$(1-\alpha)^n$
4	Phase boundary reaction	$2(1-\alpha)^{1/2}$
5	Phase boundary reaction	$3(1-\alpha)^{2/3}$
6	One-dimensional diffusion	$1/2\alpha$
7	Two-dimensional diffusion	$[-\ln(1-\alpha)]^{-1}$
8	Three-dimensional diffusion	$1.5(1-\alpha)^{2/3}\cdot[1-(1-\alpha)^{1/3}]^{-1}$
9	Four-dimensional diffusion	$1.5[(1-\alpha)^{-1/3}-1]^{-1}$
10	Prout–Tompkins equation	$\alpha(1-\alpha)$
11	Extended Prout–Tompkins equation	$\alpha^m(1-\alpha)^n$
12	Product autocatalytic primary reactions	$(1-\alpha)(1+\alpha K_{cat})$
13	Product autocatalytic n-stage reactions	$(1-\alpha)^n(1+K_{cat})$
15	Composite autocatalytic reaction	$(1-\alpha)^n(1+\alpha^m K_{cat})$
16	Two-dimensional nucleation and growth	$(1-\alpha)[-\ln(1-\alpha)]^{1/2}$
17	Three-dimensional nucleation and growth	$3(1-\alpha)[-\ln(1-\alpha)]^{2/3}$
18	N-dimensional nucleation and growth	$n(1-\alpha)[-\ln(1-\alpha)]^{n-1/n}$

K_{cat} is the autocatalytic coefficient; n and m are the order of reaction

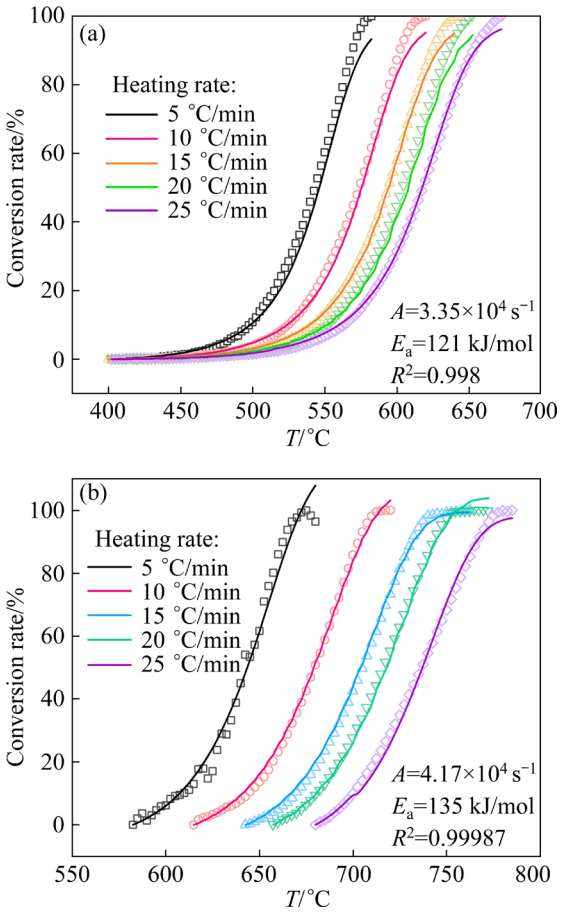

Fig. 9 Fitting results of relationship between conversion rate and temperature obtained by using kinetic equations at various heating rates: (a) First stage; (b) Second stage

Composite autocatalysis is a combination of the order reaction and an autocatalytic reaction. For the order reaction, the reaction rate decreases with the consumption of reactants. The typical characteristic of the autocatalytic reaction is the acceleration effect of products during the reaction, i.e., the conversion rate increases with increasing amount of products. In turn, the autocatalytic coefficient K_{cat} in the mechanism function of the composite autocatalysis reflects the contribution of the autocatalytic reaction.

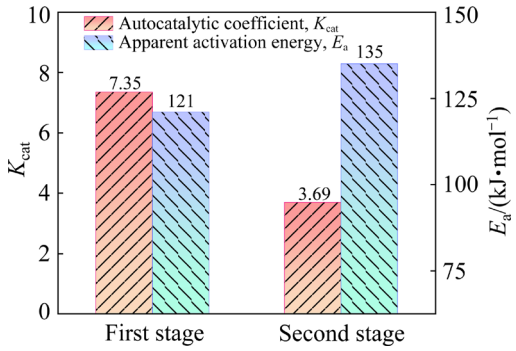

Fig. 10 Apparent activation energy and autocatalytic coefficient of hydrogen reduction of tungsten oxide during composite autocatalysis

A sequence of $WO_3 \rightarrow WO_{2.90} \rightarrow WO_{2.72} \rightarrow WO_2 \rightarrow W$ transformations can be considered as the autocatalytic reaction owing to the acceleration effect of intermediate products ($WO_{2.72}$, $WO_{2.90}$ and W) during the reduction process. At the initial stage, the reaction is in the "incubation state", where the autocatalytic acceleration effect is not obvious because of the formation of a small quantity of products. Once the reaction proceeds, it enters the "acceleration state", in which the increase in the amount of the intermediate products promotes reduction. The consumption of the intermediate products contributes to a "deceleration state". The "incubation–acceleration–deceleration" phases of $WO_3 \rightarrow WO_{2.90} \rightarrow WO_{2.72} \rightarrow WO_2 \rightarrow W$ transformations conform to the characteristic of the autocatalysis. When the reactants are consumed to a certain extent, the catalytic effect of the intermediate products is limited due to the decrease in the amount of reactants interacting with these products. Under this condition, the reduction reaction can even be converted into an order reaction.

Figure 11 shows that the aforementioned two processes pass concurrently during the hydrogen reduction of WO_3. Different contribution degrees

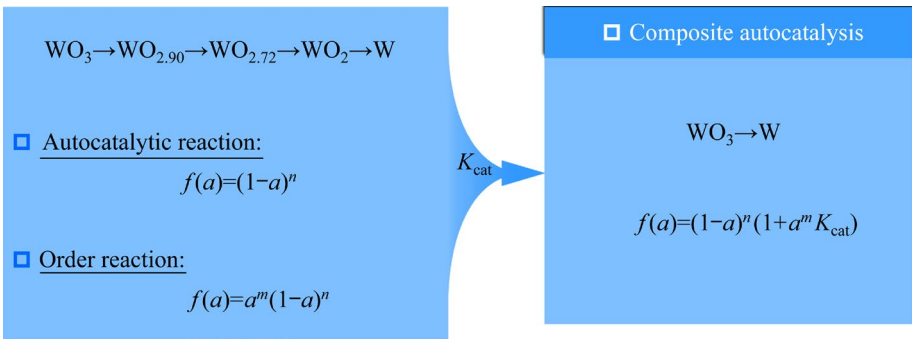

Fig. 11 Schematic diagram of composite autocatalytic reaction during hydrogen reduction of tungsten oxide

of the autocatalytic reaction in the composite autocatalysis divide the hydrogen reduction of WO_3 into two stages. In the first stage, the primary process is the autocatalytic reaction. Therefore, the autocatalytic coefficient K_{cat} in the first stage is higher than that in the second stage, as shown in Fig. 10. Finally, the corresponding conversion rates of the two stages can be expressed as follows:

First stage:

$$\frac{d\alpha}{dt} = 3.35\times10^4(1-\alpha)^{1.114}\cdot(1+7.35\alpha^{1.063})\cdot \exp[-121/(RT)] \quad (7)$$

Second stage:

$$\frac{d\alpha}{dt} = 4.17\times10^4(1-\alpha)^{10.787}\cdot(1+3.69\alpha^{0.842})\cdot \exp[-135/(RT)] \quad (8)$$

4 Conclusions

(1) The particle morphology of tungsten powders prepared under the present experimental condition was consistent with that of the WO_3 raw material, exhibiting a porous structure composed of fine tungsten grains. In turn, the tungsten powder produced via the chemical vapor deposition exhibited the polyhedral single-crystal structure.

(2) The hydrogen reduction of the tungsten oxides under the local gas–solid reduction mechanism can be described by using the composite autocatalytic reaction function. The contribution discrepancy of the autocatalytic reaction in the composite autocatalytic mechanism divides the hydrogen reduction process of WO_3 into two stages.

(3) The contribution of autocatalysis in the first stage is greater than that in the second stage, which is evident from the activation energies of 121 and 135 kJ/mol, respectively. The corresponding conversion rates for the two stages were obtained.

CRediT authorship contribution statement

Rui-fang WANG: Methodology, Validation, Investigation, Writing − Original draft, Review & editing, Project administration; **Xiang ZHAN:** Methodology, Validation, Investigation, Visualization; **Yong-qiang CHEN:** Methodology, Validation, Investigation; **Shi-ming ZHANG:** Methodology, Investigation, Writing − Review & editing; **Yu-si CHE:** Supervision, Conceptualization, Project administration; **Ji-lin HE:** Supervision, Project administration, Methodology.

Declaration of competing interest

The authors declare that they have no known competing financial interests or personal relationships that could have appeared to influence the work reported in this paper.

Acknowledgments

This work was supported by the National Key Research & Development Program of China (No. 2022YFC2904905), the National Natural Science Foundation of China (No. 52274400), the Project of Zhongyuan Critical Metals Laboratory, China (No. GJJSGFZD202302), and the Science and Technology Project of Henan Province, China (No. 232102230044).

References

[1] SUN Guo-dong, WANG Kai-fei, SONG Cheng-min, ZHANG Guo-hua. A low-cost, efficient, and industrially feasible pathway for large scale preparation of tungsten nanopowders [J]. International Journal of Refractory Metals and Hard Materials, 2019, 78: 100−106.

[2] SINGLA G, SINGH K, PANDEY O P. Structural and thermal properties of in-situ reduced WO_3 to W powder [J]. Powder Technology, 2013, 237: 9−13.

[3] REN C, FANG Z Z, ZHANG H, KOOPMAN M. The study on low temperature sintering of nano-tungsten powders [J]. International Journal of Refractory Metals and Hard Materials, 2016, 61: 273−278.

[4] WANG Xu, QIN Wen-qing, JIAO Fen, DONG Liu-yang, GUO Jian-gen, ZHANG Jian, YANG Cong-ren. Review of tungsten resource reserves, tungsten concentrate production and tungsten beneficiation technology in China [J]. Transactions of Nonferrous Metals Society of China, 2022, 32(7): 2318−2338.

[5] YI Zhi-qiang, TAN Dun-qiang. Refining mechanisms of arsenic during preparation process of ultrafine WC powder by nitridation−carbonization method [J]. Transactions of Nonferrous Metals Society of China, 2024, 34(3): 966−976.

[6] WANG Kai-fei, ZHANG Guo-hua. Synthesis of high-purity ultrafine tungsten and tungsten carbide powders [J]. Transactions of Nonferrous Metals Society of China, 2020, 30(6): 1697−1706.

[7] LI Bao-qiang, SUN Zhi-qiang, HOU Guo-lin, DING Fei, HU Peng, YUAN Fang-li. The sintering behavior of quasi-spherical tungsten nanopowders [J]. International Journal of Refractory Metals and Hard Materials, 2016, 56: 44−50.

[8] SARMAH T, AOMOA N, BHATTACHARJEE G, SARMA S, BORA B, SRIVASTAVA D N, BHUYAN H, KAKATI M, de

TEMMERMAN G. Plasma expansion synthesis of tungsten nanopowder [J]. Journal of Alloys and Compounds, 2017, 725: 606−615.

[9] CETINKAYA S, EROGLU S. Thermodynamic analysis and reduction of tungsten trioxide using methane [J]. International Journal of Refractory Metals and Hard Materials, 2015, 51: 137−140.

[10] WU Xiang-wei, LUO Jing-song, LU Bi-zhi, XIE Chen-hui, PI Zhi-ming, HU Mao-zhong, XU Tao, WU Guo-gen, YU Zhi-ming, YI Dan-qing. Crystal growth of tungsten during hydrogen reduction of tungsten oxide at high temperature [J]. Transactions of Nonferrous Metals Society of China, 2009, 19(3): 785−789.

[11] ZHANG Hai-bao, BAI Liu-yang, HU Peng, YUAN Fang-li, LI Jin-lin. Single-step pathway for the synthesis of tungsten nanosized powders by RF induction thermal plasma [J]. International Journal of Refractory Metals and Hard Materials, 2012, 31: 33−38.

[12] LI Heng-li, SHANG Hui-jun, PAN Feng, LI Wei-jun, DU Zhan. Preparation of ultrafine tungsten powder by fluidized bed hydrogen reduction of WO_3−Co_3O_4 [J]. International Journal of Refractory Metals and Hard Materials, 2024, 120: 106607.

[13] SCHUBERT W D, LASSNER E. Production and characterization of hydrogen-reduced submicron tungsten powders. Part II: Controlled decomposition of APT and hydrogen reduction of the oxides [J]. International Journal of Refractory Metals and Hard Materials, 1991, 10(4): 171−183.

[14] WU Chong-hu. Preparation of ultrafine tungsten powders by in-situ hydrogen reduction of nano-needle violet tungsten oxide [J]. International Journal of Refractory Metals and Hard Materials, 2011, 29(6): 686−691.

[15] SONG Han-lin, JIANG Ping-guo, LIU Wen-jie, WANG Zheng-bing. Research progress on hydrogen reduction kinetics of tungsten oxide [J]. Nonferrous Metals Science and Engineering, 2017, 8(5): 64−69. (in Chinese)

[16] JIANG Ping-guo, XIAO Yi-yu, YU Xiang-biao, LI Rong-bin. Research progress in hydrogen reduction mechanism of tungsten oxide [J]. The Chinese Journal of Nonferrous Metals, 2022, 32(2): 520−528. (in Chinese)

[17] GUO Feng. Research status of preparing ultrafine tungsten powders by H_2-reducing tungsten oxide [J]. Materials Science and Engineering of Powder Metallurgy, 2007, 12(4): 205−210. (in Chinese)

[18] ZIMMERL T, SCHUBERT W D, BICHERL A, BOCK A. Hydrogen reduction of tungsten oxides: Alkali additions, their effect on the metal nucleation process and potassium bronzes under equilibrium conditions [J]. International Journal of Refractory Metals and Hard Materials, 2017, 62: 87−96.

[19] LI Meng-chao, WANG Lu, XUE Zheng-liang. Kinetic and mechanism study of the reduction of WO_2 to W by CO or CO−CO_2 mixed gas [J]. JOM, 2023, 75(9): 3951−3961.

[20] WU Yi-jie, LU Ze-peng, SUN Hai-bo, DANG Jie. Production of different morphologies and size of metallic W particles through hydrogen reduction [J]. Journal of Materials Research and Technology, 2019, 8(5): 4687−4698.

[21] LÜ Ze-peng, JIAN Kai-liang, DANG Jie. Effect of salt-assisted reduction method on morphologies and size of metallic tungsten particles [J]. Transactions of Nonferrous Metals Society of China, 2020, 30(11): 3133−3146.

[22] SCHODERBÖCK P. The reduction of tungsten-VI-oxide to tungsten: A thermogravimetric microscale study with focus on the intermediates [J]. Thermochimica Acta, 2022, 707: 179113.

[23] WANG Rui-fang, ZHAN Xiang, CHEN Yong-qiang, ZHANG Chao, CHE Yu-si, HE Ji-lin. Regulation of particle size and morphology of tungsten powders in bottom-blowing hydrogen reduction process [J]. International Journal of Refractory Metals and Hard Materials, 2024, 118: 106495.

[24] CHEN Yong-qiang, YANG Rui-rui, ZHANG Chao, SONG Jian-xun, CHE Yu-si, HE Ji-lin. Novel process for preparing tungsten powder by hydrogen reduction of tungsten trioxide [J]. International Journal of Refractory Metals and Hard Materials, 2022, 106: 105869.

[25] OSTERMANN M, DALBAUER V, SCHUBERT W D, HAUBNER R. Preparation of nano-crystalline tungsten powders from gaseous $WO_2(OH)_2$ [J]. Tungsten, 2022, 4(1): 60−66.

[26] ZAKI M I, FOUAD N E, MANSOUR S A A, MUFTAH A I. Temperature-programmed and X-ray diffractometry studies of hydrogen-reduction course and products of WO_3 powder: Influence of reduction parameters [J]. Thermochimica Acta, 2011, 523(1/2): 90−96.

[27] ESTUPINAN-DONOSO A A, GRAVIER P, ICHIKAWA R U, MICHELS A. Unraveling grain growth of metallic tungsten: Investigating the nanoscale realm of hydrogen reduction of tungsten oxides [J]. Powder Technology, 2024, 438: 119672.

[28] CHE Yu-si, HAO Zhen-hua, ZHU Jin-peng, FU Zhen-hua, HE Ji-lin, SONG Jian-xun. Kinetic mechanism of magnesium production by silicothermy in argon flowing [J]. Thermochimica Acta, 2019, 681: 178397.

[29] PANG Yue-peng, LI Qian. A review on kinetic models and corresponding analysis methods for hydrogen storage materials [J]. International Journal of Hydrogen Energy, 2016, 41(40): 18072−18087.

[30] CHE Yu-si, ZHANG Chao, SONG Jian-xun, SHANG Xiao-jia, CHEN Xi-ping, HE Ji-lin. The silicothermic reduction of magnesium in flowing argon and numerical simulation of novel technology [J]. Journal of Magnesium and Alloys, 2020, 8(3): 752−760.

[31] ZHANG Yu-juan, GUO Xin-tao, WANG Chun-hong, WU De-feng. Self-polymerization and co-polymerization kinetics of lead methacrylate [J]. Rare Metals, 2021, 40(3): 736−742.

[32] LIU Peng-yuan, WANG Hong, WANG Zhen-qiang, QIU Yu-qing, CHEN Xing-yu, SUN Feng-long, CHEN Ai-liang, LIU Xu-heng, LI Jiang-tao, ZHAO Zhong-wei. Kinetics study on selective dissolution of tungsten from scheelite acid decomposition residue [J]. The Chinese Journal of Nonferrous Metals, 2023, 33(8): 2666−2677. (in Chinese)

非等温过程中三氧化钨的氢还原动力学及其形貌演变机制

王瑞芳[1,2,3]，詹 翔[1,2]，陈永强[1,2]，张石明[1,2]，车玉思[1,2,3]，何季麟[1,2,3]

1. 郑州大学 中原关键金属实验室，郑州 450001；
2. 郑州大学 稀有金属特种材料全国重点实验室，郑州 450001；
3. 郑州大学 材料科学与工程学院，郑州 450001

摘 要：采用非等温热重分析法研究了 WO_3 氢还原的动力学。在局部气−固还原条件下，钨粉颗粒形貌与原料 WO_3 的保持一致。钨氧化物中氧的脱除导致氢还原产物颗粒形成多孔结构，与化学气相沉积条件下制得的单晶多面体钨粉存在明显差异。此外，在局部气−固还原条件下，WO_3 氢还原过程中两个阶段均可用复合自催化函数描述，其第一、二阶段的反应活化能分别为 121 和 135 kJ/mol。

关键词：三氧化钨；钨粉；氢还原；反应动力学；颗粒形貌

(Edited by Wei-ping CHEN)